Nicolas Riesen, Xuanzhao Pan, Kate Badek, Yinlan Ruan, Tanya M. Monro, Jiangbo Zhao, Heike Ebendorff-Heidepriem, and Hans Riesen

Towards rewritable multilevel optical data storage in single nanocrystals

Optics Express, 2018; 26(9):12266-12276

DOI: http://dx.doi.org/10.1364/OE.26.012266

Research Article | Vol. 26, No. 9 | 30 Apr 2018 | OPTICS EXPRESS 12266
Optics EXPRESS

Towards rewritable multilevel optical data storage in single nanocrystals

NICOLAS RIESEN,[1,2,4,*] XUANZHAO PAN,[2,4] KATE BADEK,[3] YINLAN RUAN,[2] TANYA M. MONRO,[1,2] JIANGBO ZHAO,[2] HEIKE EBENDORFF-HEIDEPRIEM,[2] AND HANS RIESEN[3]

[1]*University of South Australia and Future Industries Institute, Mawson Lakes, SA 5095, Australia*
[2]*Institute for Photonics and Advanced Sensing (IPAS) and School of Physical Sciences, The University of Adelaide, SA 5005, Australia*
[3]*School of Physical, Environmental and Mathematical Sciences, The University of New South Wales, Canberra, ACT 2600, Australia*
[4]*These authors contributed equally*
**nicolas.riesen@unisa.edu.au*

Abstract: Novel approaches for digital data storage are imperative, as storage capacities are drastically being outpaced by the exponential growth in data generation. Optical data storage represents the most promising alternative to traditional magnetic and solid-state data storage. In this paper, a novel and energy efficient approach to optical data storage using rare-earth ion doped inorganic insulators is demonstrated. In particular, the nanocrystalline alkaline earth halide BaFCl:Sm is shown to provide great potential for multilevel optical data storage. Proof-of-concept demonstrations reveal for the first time that these phosphors could be used for rewritable, multilevel optical data storage on the physical dimensions of a single nanocrystal. Multilevel information storage is based on the very efficient and reversible conversion of Sm^{3+} to Sm^{2+} ions upon exposure to UV-C light. The stored information is then read-out using confocal optics by employing the photoluminescence of the Sm^{2+} ions in the nanocrystals, with the signal strength depending on the UV-C fluence used during the write step. The latter serves as the mechanism for multilevel data storage in the individual nanocrystals, as demonstrated in this paper. This data storage platform has the potential to be extended to 2D and 3D memory for storage densities that could potentially approach petabyte/cm^3 levels.

OCIS codes: (160.4236) Nanomaterials; (160.5690) Rare-earth-doped materials; (210.0210) Optical data storage; (210.4810) Optical storage-recording materials; (250.5230) Photoluminescence; (300.6250) Spectroscopy, condensed matter.

References and links

1. M. Hilbert and P. López, "The world's technological capacity to store, communicate, and compute information," Science **332**(6025), 60–65 (2011).
2. J. Gantz and D. Reinsel, *The Digital Universe in 2020: Big Data, Bigger Digital Shadows, and Biggest Growth in the Far East.* Framingham, MA: IDC 2012. Available from: https://www.emc.com/collateral/analyst-reports/idc-the-digital-universe-in-2020.pdf.
3. A. M. Earman, "Optical data storage with electron trapping materials using M-ary data channel coding," in *Optical Data Storage Topical Meeting*, (SPIE, 1992), pp. 92–103.
4. S. Dhomkar, J. Henshaw, H. Jayakumar, and C. A. Meriles, "Long-term data storage in diamond," Sci. Adv. **2**(10), e1600911 (2016).
5. J. Zhang, M. Gecevičius, M. Beresna, and P. G. Kazansky, "Seemingly unlimited lifetime data storage in nanostructured glass," Phys. Rev. Lett. **112**(3), 033901 (2014).
6. M. Savoini, P. Biagioni, L. Duò, and M. Finazzi, "All-optical subdiffraction multilevel data encoding onto azo-polymeric thin films," Opt. Lett. **34**(6), 761–763 (2009).
7. D. Ganic, D. Day, and M. Gu, "Multi-level optical data storage in a photobleaching polymer using two-photon excitation under continuous wave illumination," Opt. Lasers Eng. **38**(6), 433–437 (2002).
8. H.-P. D. Shieh, Y.-L. Chen, and C.-H. Wu, "Multilevel recording in erasable phase-change media by light intensity modulation," Jpn. J. Appl. Phys. **40**(Part 1, No. 3B), 1850–1854 (2001).

#326419 https://doi.org/10.1364/OE.26.012266
Journal © 2018 Received 20 Mar 2018; revised 16 Apr 2018; accepted 17 Apr 2018; published 26 Apr 2018

Optics EXPRESS

9. Y. Tang, J. Pei, Y. Ni, L. Pan, H. Hu, and B. Zhang, "Multi-level read-only recording using signal waveform modulation," Opt. Express **16**(9), 6156–6162 (2008).
10. Y. Hu, Z. Zhang, Y. Chen, Q. Zhang, and W. Huang, "Two-photon-induced polarization-multiplexed and multilevel storage in photoisomeric copolymer film," Opt. Lett. **35**(1), 46–48 (2010).
11. Y. Hu, D. Wu, J. Li, W. Huang, and J. Chu, "Two-stage optical recording: photoinduced birefringence and surface-mediated bits storage in bisazo-containing copolymers towards ultrahigh data memory," Opt. Express **24**(20), 23557–23565 (2016).
12. H. Hagemann, V. D'Anna, M. Lawson Daku, and F. Kubel, "Crystal chemistry in the barium fluoride chloride system," Cryst. Growth Des. **12**(3), 1124–1131 (2012).
13. R. Jaaniso and H. Bill, "High-temperature spectral hole burning on Sm-doped single crystal materials of PbFCl family," J. Lumin. **64**(1-6), 173–179 (1995).
14. R. Jaaniso, H. Hagemann, and H. Bill, "Members of the PbFCI-type family: possible candidates for room-temperature photochemical hole burning," CHIMIA Intern. J. Chem. **46**, 133–137 (1992).
15. H. Bill, R. Jaaniso, H. Hagemann, D. Lovy, A. Monnier, and M. Schnieper, "High-temperature spectral hole burning on samarium (II) in single crystals of the lead fluorohalide structure family and in thin films of calcium fluoride," Opt. Eng. **34**(8), 2333–2338 (1995).
16. W. Moerner, W. Lenth, and G. Bjorklund, "Frequency domain optical storage and other applications of persistent spectral hole-burning," in *Persistent Spectral Hole-Burning: Science and Applications* (Springer, 1988), pp. 251–307.
17. J. Qiu, K. Miura, T. Suzuki, T. Mitsuyu, and K. Hirao, "Permanent photoreduction of Sm^{3+} to Sm^{2+} inside a sodium aluminoborate glass by an infrared femtosecond pulsed laser," Appl. Phys. Lett. **74**(1), 10–12 (1999).
18. X. Xu, X. Yu, T. Wang, W. Bian, and J. Qiu, "Rewritable LPL in Sm^{3+}-doped borate glass with the assistance of defects induced by femtosecond laser," Opt. Mater. Express **6**(2), 402–408 (2016).
19. H. Riesen, K. Badek, T. M. Monro, and N. Riesen, "Highly efficient valence state switching of samarium in BaFCl:Sm nanocrystals in the deep UV for multilevel optical data storage," Opt. Mater. Express **6**(10), 3097–3108 (2016).
20. Z. Liu, M. Stevens-Kalceff, and H. Riesen, "Photoluminescence and cathodoluminescence properties of nanocrystalline BaFCl:Sm^{3+} X-ray storage phosphor," J. Phys. Chem. C **116**(14), 8322–8331 (2012).
21. E. Radzhabov and V. Otroshok, "Optical spectra of oxygen defects in BaFCl and BaFBr crystals," J. Phys. Chem. Solids **56**(1), 1–7 (1995).
22. H. Riesen and W. A. Kaczmarek, "Efficient X-ray generation of Sm^{2+} in nanocrystalline BaFCl/Sm^{3+}: a photoluminescent X-ray storage phosphor," Inorg. Chem. **46**(18), 7235–7237 (2007).
23. T. Smeeton, K. Welna, E. Boardman, R. Pereira, and V. Berryman-Bousquet, "Compact UVC laser shows promise for environmental sensing," Photon. Spectra **51**, 40–44 (2017).
24. Y. Hu, J. Ma, Y. Chen, J. Li, W. Huang, and J. Chu, "Fast bits recording in photoisomeric polymers by phase-modulated femtosecond laser," IEEE Photonics Technol. Lett. **26**(11), 1154–1156 (2014).
25. X. L. Wang, Z. Q. Liu, M. A. Stevens-Kalceff, and H. Riesen, "Mechanochemical preparation of nanocrystalline BaFCl doped with samarium in the 2+ oxidation state," Inorg. Chem. **53**(17), 8839–8841 (2014).
26. Z. Liu, M. A. Stevens-Kalceff, X. Wang, and H. Riesen, "Mechanochemical synthesis of nanocrystalline BaFCl: Sm^{3+} storage phosphor by ball milling," Chem. Phys. Lett. **588**, 193–197 (2013).
27. A. N. Shipway, M. Greenwald, N. Jaber, A. M. Litwak, and B. J. Reisman, "A new medium for two-photon volumetric data recording and playback," Jpn. J. Appl. Phys. **45**(2B), 1229–1234 (2006).

1. Introduction

There is a growing need to massively increase data storage capacities as they are rapidly outpaced by the exponential growth in data generation [1, 2]. In particular, data generation has grown at least 3-times faster worldwide than data storage capacities in recent years and it is expected that by 2020, ~40 ZB (1 ZB = 10^{12} GB) of data will be generated annually [2]. It is therefore imperative that new approaches beyond traditional magnetic and solid-state data storage are developed to meet this demand. One of the most promising solutions is optical data storage which has been investigated in a variety of different approaches and using a range of different materials [3–5]. Importantly, optical data storage permits multilevel encoding [3]. Multilevel encoding allows for the storage capacity to be increased by writing more than one bit per point. This approach is possible when the signal-to-noise ratio (SNR) of the measured response from a pixel is high and the physical property that undergoes the photoinduced change has a large dynamic range. Importantly, multilevel data storage also increases the data transfer rate as several bits are read-out simultaneously, which is particularly important for big data. Multilevel encoding has been demonstrated for instance in polymers but it appears that these systems are subject to significant bleaching with limited number of levels and linearity [6, 7]. Multilevel encoding has also previously been

Optics EXPRESS

demonstrated in optical discs for up to 2 bits per point storage [8, 9] and in photoisomeric birefringent polymers using high power femtosecond lasers for the write step [10, 11].

In this paper multilevel optical data storage is approached in an innovative way by using inorganic insulator nanocrystals doped with rare-earth ions, namely the alkaline earth halide BaFCl:Sm^{3+}. The BaFCl host crystallizes in the tetragonal matlockite (PbFCl) structure with P4/nmm space group [12]. Matlockites doped with Sm^{2+} have generated significant interest over the last decades since these systems allow for the rare phenomenon of spectral hole-burning at room temperature [13–15], a phenomenon which itself could be exploited as an extra dimension for data storage in the frequency domain [16]. We note that samarium doped glasses have previously been employed for write-once binary optical data storage but such demonstrations have required high power femtosecond lasers [17, 18]. The investigation presented here relies on our discovery of extremely efficient and reversible valence state conversion ($Sm^{3+}\rightarrow Sm^{2+}$) within BaFCl:$Sm^{3+}$ upon excitation into transitions in the UV-C region (~215-180 nm) of oxide impurities in the host. The generated Sm^{2+} can then be read-out by the sharp *f-f* fluorescence lines [19]. In this paper, we provide for the first time a proof-of-concept of reversible *multilevel* optical data storage approaching the level of a single nanocrystal. The multilevel encoding can be achieved by discretizing the level of valence state switching by adjusting the UV-C intensity for the conversion, with the fluorescence intensity read-out using confocal optics. This paper provides a demonstration of the complete write-read-erase cycle and concludes by predicting the potential storage capacities achievable in 2D and 3D media using this platform.

2. Experimental

A. BaFCl:Sm nanocrystals

The nanocrystalline BaFCl:Sm^{3+} was prepared by co-precipitation as has been described previously [20]. In brief, 25 mL of a 0.2 M aqueous solution of NH_4F was added to 25 mL of a 0.4 M aqueous $BaCl_2$ solution containing 0.6 mg of $SmCl_3{\cdot}6H_2O$. The co-precipitation results in nanocrystals with platelet morphology with a typical size of ~300 × 200 × 50 nm [20]. We note that oxygen impurities in matlockites, MeFCl with Me = Ba, Sr, are ubiquitous, and it is hence difficult to prepare oxide free BaFCl [19, 21]. Naturally, it is anticipated that in nanocrystalline BaFCl prepared by co-precipitation the concentration of oxide impurities is relatively high because of the large surface to volume ratio [19]. Note however that in contrast to the x-ray storage phenomenon in BaFCl:Sm^{3+} [22], the optical storage effect that is based on oxygen impurities used here does not require the presence of barium for high efficiencies so other hosts, such as SrFCl and CaFCl, could be used for optical data storage. Upon excitation into the broad O^{2-} transitions around 200 nm, an electron from the oxide impurity in the BaFCl host is transferred to Sm^{3+}, yielding relatively stable Sm^{2+} centers. Since the average separation of the oxide impurity-samarium ion is ~10 Å (i.e. a few interionic separations) backtransfer of the electron after two-photon ionization is prevented [19]. The Sm^{2+} can be read-out by the very narrow and intense ^5D_J-^7F_J *f-f* luminescence lines in the red region of the visible spectrum. Importantly, these transitions can be efficiently excited via the parity allowed $4f^6\rightarrow 4f^5 5d^1$ transition (~400 l/(mol·cm)) at a wavelength of 420 ± 20 nm using inexpensive blue-violet laser diodes. Note, the fluorescence of Sm^{2+} is far more intense because the broad *f-d* absorption around 425 nm is more than two orders of magnitude stronger than the *f-f* absorption of Sm^{3+} at 401 nm.

To disperse the BaFCl crystals onto a substrate for the measurements, an agglomeration-free suspension in dichloromethane (DCM) was first created. Dispersing the crystals in DCM (1 mg/ mL) involved agitating the solution for approximately 1 minute and ultrasonicating for 18 hours. The solution was then centrifuged at 4000 rpm for 5 minutes and the supernatant extracted. The BaFCl nanocrystals were then deposited onto alphabetically-marked silicon wafers that, before the application, were rigorously cleaned in ultrasonic baths. The

Optics EXPRESS

deposition was done using 3 µL droplets of the supernatant. The samples were subsequently placed in an oven at 80 °C for 30 minutes to remove any trace of the solvent. The silicon wafers (1 cm × 1cm) were custom inscribed with alphabetic letters using deep reactive ion etching, which would facilitate tracking of individual nanocrystals during the various processing steps in which the wafers were removed from the confocal setup.

B. Experimental setups

The fluorescence read-out measurements were performed with confocal optics, mainly so that the signal from an individual crystal could be isolated. Confocal optics is also important for rapid read-out because the $^5D_0$ excited state of Sm^{2+}, from which the fluorescence originates, has a relatively long excited state lifetime of ~2 ms [22]. Using confocal optics ensures that the fluorescence from only one pixel is observed at any given time, i.e. the remaining fluorescence from the previous pixels is not picked up. The basic scanning confocal microscope (SCM) used for both the read-out and erase steps was a custom-built system shown in the schematic of Fig. 1. It consisted of a fiber-coupled 405 nm diode laser (CrystaLaser, DL405-025) as the source, an XYZ Nanopositioning stage (PInano, P-545.3R8S) with 100 × /0.90 objective (Nikon, TU Plan Apo) and a controller programmed with LabVIEW for the scan. The laser spot size was < 1 µm. We note here that the optical pick-up (OPU) of e.g. BD and DVD players is essentially in the same confocal arrangement and so a reader closely resembling these well-established consumer technologies could in principle be used for compact 2D read-out.

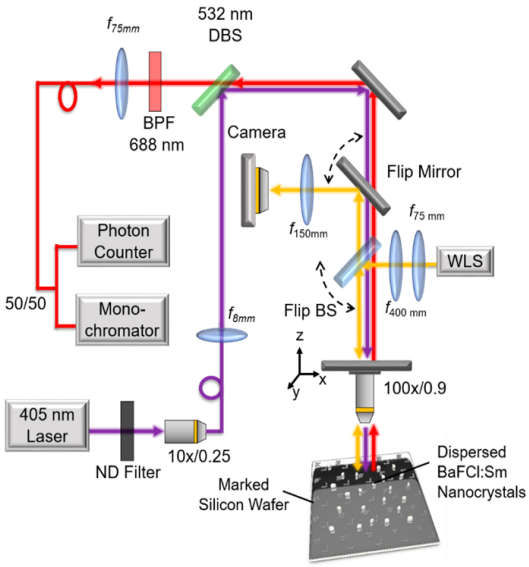

Fig. 1. Experimental setup with custom scanning confocal microscope arrangement for read-out. Solid lines represent fibers, glowing lines are free-space propagation. BPF: Bandpass filter, BS: Beamsplitter, DBS: Dichroic beamsplitter, WLS: White light source.

The excitation and emission light was separated using a 532 nm dichroic beamsplitter. The SCM fluorescence images were collected using a fiber-coupled solid state single photon counter (Excelitas, SPCM-AQRH), and the spectra were measured with a monochromator (Horiba, iHR320) equipped with a 300 groove/mm, 600 nm blazed grating and a cooled CCD (Horiba, Synapse 1024 × 256 pixels). A 50:50 multimode fiber (200 µm diameter) coupler was used to split light to both the photon counter and monochromator. To eliminate background fluorescence and to isolate the dominant ~688 nm peak of the converted BaFCl:Sm^{2+} ($^5D_0 \rightarrow {}^7F_0$), which can be overpowered by the Sm^{3+} background fluorescence, a

Optics EXPRESS

custom-made narrow bandpass filter (Andover, 687.8 nm; 1 nm bandpass) was used for the SCM imaging. To assist with locating and focusing on the nanocrystals on the marked silicon wafers, the samples were illuminated with a white light LED source (Thorlabs, MCWHL2) and viewed on a high-performance cooled digital microscope camera (Nikon DS-Qi1). This auxiliary setup relied on a flip beamsplitter and flip mirror as shown in Fig. 1. The samples were converted ($Sm^{3+}\rightarrow Sm^{2+}$) by exposure to a UV lamp (Rexim, LLC UV-C Cold Cathode Lamp MCCUV-C, ~50 μW/cm^2 at 185 nm and 100 mm distance) placed on top of the sample after it was removed from the scanning confocal microscope. Ideally, UV-grade optics and a UV-C laser (e.g. second harmonic of a 415 nm laser diode) would allow for the writing to be performed on the scanning confocal microscope without sample removal. The read-out at 405 nm was performed at low powers (~50 μW), with erasure of the signal achieved without sample removal by increasing the laser power (~220 μW) whilst fixing the confocal microscope on the particular point. The nanocrystals were also characterized with Scanning Electron Microscopy (FEI, Quanta 450 FEG, 10 kV), with these measurements performed last to avoid valence state and structural changes due to the electron beam.

3. Results & Discussion

A. Scanning confocal microscope read-out

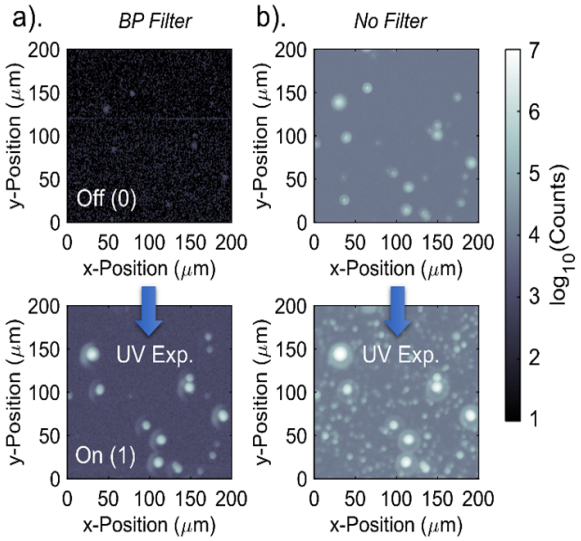

Fig. 2. SCM images (200 × 200 μm^2) of dispersed BaFCl:Sm^{3+} nanocrystals before and after UV-C (185 nm, t >10 mins, P~200 μW/cm^2) exposure (a) with and (b) without 687.8 nm, 1 nm bandpass (BP) filter, respectively.

SCM images of the dispersed BaFCl:Sm^{3+} nanocrystals are shown in Fig. 2 before and after UV-C exposure when using (a) the 687.8 nm bandpass (BP) filter and (b) no filter. This figure clearly confirms the importance of filtering out the residual fluorescence originating mainly from the Sm^{3+}. This is crucial to allow for discernible 'Off' and 'On' nanocrystal states and improving the SNR (e.g. reducing the background fluorescence) for multilevel encoding. The 687.8 nm narrowband filter which isolates the dominant $^5D_0\rightarrow{}^7F_0$ transition of Sm^{2+} is used for all subsequent SCM images presented in this paper. The use of this filter also demonstrates that the read-out can be performed by simply using intensity measurements rather than spectral analysis. In these measurements, the samples were removed from the setup during the valence state switching/writing ($Sm^{3+}\rightarrow Sm^{2+}$) with exposure to the UV lamp. The writing speed in the experiments was greatly limited by the very low UV-C power (185 nm) available from the mercury lamp. Importantly, much faster write speeds would be

Optics EXPRESS

enabled by employing a laser in the 215-180 nm region, e.g. a 193 nm ArF excimer laser (see below for an example) or a frequency-doubled blue-violet laser diode [23]. We estimate that to completely saturate a nanocrystal ~200 nm^3 in size, a mere 24 pJ of energy would be required [19]. The fluorescence read-out was done at 50 µW (measured above the SCM objective). The read-out speed in the experiments was limited by the basic 2D XY scan implemented. The read speed was slow at 10 minutes for a 200 × 200 μm^2 area. In practice, however, it is expected that the read speed could exceed that of Blu-ray™ technology by at least a factor equal to the number of bits in the multilevel encoding when employing a similar technology.

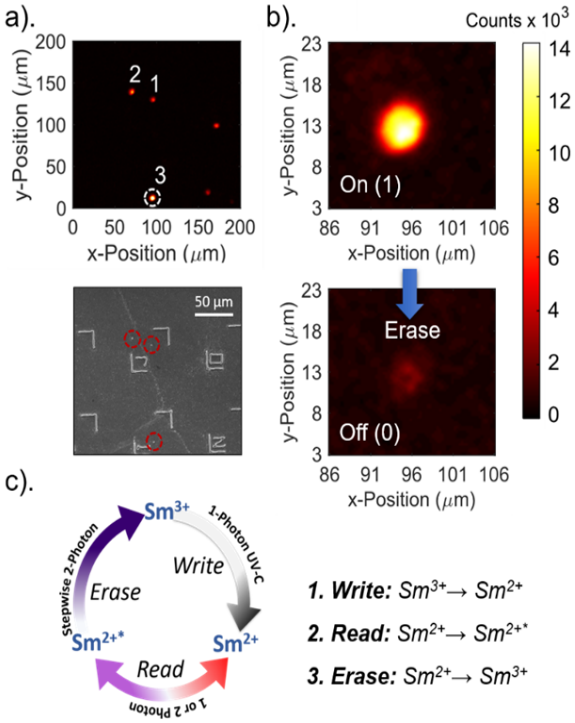

Fig. 3. Nanocrystal bleaching/erasure demonstration. (a) SCM image of BaFCl:Sm^{3+} nanoaggregates of 2-3 crystals C_1, C_2 and C_3 after exposure to UV-C (λ ~185 nm, *t* >10 mins, *P*~200 µW/cm^2) and corresponding SEM (ETD) image. (b) Subsequent On-Off state erasure (λ = 405 nm, *P* = 220 µW) of C_3 (with read-out λ_{ex} = 405 nm, *P* = 50 µW, λ_{em} = 687.8 nm, $^5D_0 \rightarrow {}^7F_0$). (c). Schematic of write-read-erase mechanism for BaFCl:Sm.

We note however that the excited state lifetime of the fluorescence will ultimately limit the read rate since it limits the number of photons observed during the dwell time. Fortunately, the *d-f* transitions used for the read-out are highly efficient. We also note that multi-spot recording and reading techniques could also be adopted for further increasing the write and read times [24].

B. Nanocrystal bleaching/erasure

A second wafer was then exposed to UV-C for >10 minutes, with the SCM image read-out at low power (λ_{ex} = 405 nm, *P* = 50 µW, λ_{em} = 687.8 nm, $^5D_0 \rightarrow {}^7F_0$) as is shown in Fig. 3(a) in which three nanoaggregates of 2-3 nanocrystals C_1, C_2 and C_3 were identified. It is later shown that the write time can be reduced to nanosecond timescales using a higher-power UV laser source. It is also noted that the Sm^{2+} is indefinitely stable in the BaFCl host, unless the system is exposed to high intensity blue light, making this platform suitable for long-term data storage. Bleaching of nanoaggregate C_3 with the reverse $Sm^{3+} \rightarrow Sm^{2+}$ process is shown

Optics EXPRESS

to occur in Fig. 3(b) when increasing the read-out power at 405 nm from 50 μW to 220 μW whilst fixing the microscope on that point. This result clearly demonstrates the erasure of the dominant 688 nm fluorescence signal, providing a proof-of-concept of the erase procedure (stepwise 2-photon ionization). The power dependence of the erasure has previously been studied and dispersive first-order kinetics was observed [19]. Note that the erasure is not 100%, with a small residual signal of typically ~5% remaining just above the noise floor. This residual signal is due to Sm^{2+} ions which get stabilized within the host lattice because either the original electron donor (oxide ion) diffuses away from the samarium ion such that the donor-acceptor separation increases, or the initial Sm^{3+}-oxide pair separation inhibits back electron transfer. This build-up of Sm^{2+} centers that cannot be ionized might limit the number of erase cycles possible for the current system and more work, e.g. variations of the host material, has to be undertaken to overcome this potential constraint.

The *write-read-erase* cycle for data storage using these UV storage phosphors is summarized in Fig. 3(c). The one-photon write process (UV-C) converts the Sm^{3+} to Sm^{2+} via an electron transferred from O^{2-} impurities in the BaFCl host. The one-photon excited red photoluminescence of the Sm^{2+} is then read-out in the blue-violet. We note that the read-out process could also be conducted via two-photon absorption in the near-infrared. The erase step involves increasing the power of the blue-violet source to achieve 2-photon ionization to convert the samarium back to its original Sm^{3+} valence state.

C. Towards multilevel optical data storage

The SCM image of the same wafer, after nanoaggregates C_1, C_2 and C_3 have each in turn been bleached back to the Sm^{3+} state, is shown in Fig. 4. This time by adjusting the UV-C exposure duration (or alternatively the intensity) the level of valence state switching ($Sm^{3+} \rightarrow Sm^{2+}$) can be finely tuned even at the nanocrystal level. The coarse scan images of the three nanocrystal aggregates before exposure, and after 1 and 5 minutes of UV exposure, respectively, is shown in Fig. 4(a), demonstrating the gradual increase in intensity of the $^5D_0 \rightarrow {}^7F_0$ transition when read-out at constant power. Figure 4(b) shows finer scans of the multilevel valence state switching of the three nanoaggregates which were subsequently imaged using scanning electron microscopy (SEM) in Fig. 4(c). Note SEM imaging was performed only at the end, since the electron beam can switch the valence state of the samarium ions [20]. The nanocrystals or nanoaggregates appear larger on the SCM images due to issues with focusing on the sample. We also note here that the write time required is determined by the power of the UV source used. As shown in Fig. 4(e), this write time can be reduced by more than 10 orders of magnitude if a UV-C laser around 215-180 nm such as a 193 nm ArF excimer laser (Lambda Physik LPFpro 202) is employed instead of the low power mercury lamp. This is demonstrated for the case of a 20 mg sample. Figure 4(e) shows that after just one 30 ns laser pulse at 193 nm of ~30 mJ/cm^2 the signal level exceeds that reached after a 5 minute exposure to the UV mercury lamp used in the present work. This clearly demonstrates that data could be written on the nanosecond timescale or faster. Whilst pulsed UV lasers allow for extremely rapid write rates, a CW UV laser would also provide a dramatic reduction in the write time compared with the weak mercury lamp used, whilst being more suited to intensity modulation for the multilevel encoding.

Figure 4 has provided a proof-of-concept towards multilevel data storage using the greyscale write procedure. This demonstration has shown the write step (UV-C ~185 nm) with multilevel encoding of the data, with read-out by one-photon (blue-violet region) excited photoluminescence (red region of visible spectrum). Importantly, the read-out could in principle be conducted by exciting the red photoluminescence via two-photon absorption of near infrared light, allowing for the elimination of any potential bleaching during the read-out step. We note here that many more levels could be generated in between the three discrete intensity levels demonstrated in Fig. 4, using different UV-C exposure levels, although for a single nanocrystal the number of levels is limited by the number of Sm^{3+} ions per crystallite

Optics EXPRESS

(250 ppm samarium concentration here, as measured by using ICP-OES). Nevertheless, it can easily be envisioned that hundreds or even thousands of levels could be encoded if a sample consisting of a thin film of nanocrystals of e.g. ~10 µm thickness can be directly exposed with the confocal microscope. Importantly, BaFCl:Sm^{3+} has a large dynamic range for the Sm^{2+} signal that is induced by the photoreduction, and the growth of the Sm^{2+} signal is linear over several orders of magnitude. The dynamic range and hence the number of bits that could be encoded on a single nanocrystal in the present basic experiment is limited by the number of Sm^{3+} ions and the signal-to-noise ratio. The latter could, however, be improved significantly by eliminating background light, improving the collection efficiency especially in terms of fiber coupling and using the more efficient 420 nm excitation wavelength of Sm^{2+} [19]. There is also the possibility of using a pulsed blue-violet laser source to maximize the fluorescence signal for the read-out and avoid potential bleaching. Also, of particular importance is laser stability to ensure low noise for the multilevel read-out. This requirement could however be mitigated by a ratio-metric read-out where a Sm^{3+} transition is used as a reference.

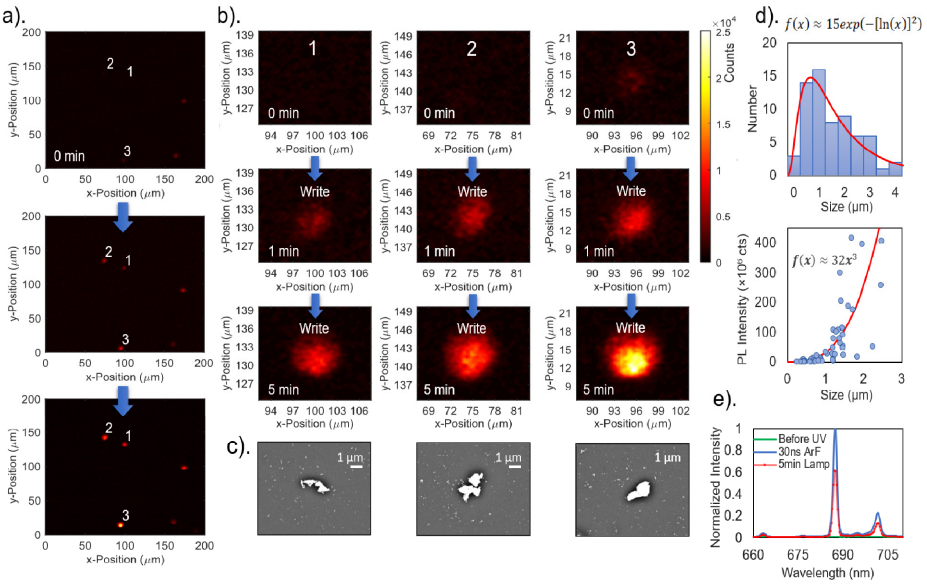

Fig. 4. Multilevel optical data storage. (a) Shown are the coarse scan SCM images (λ_{ex} = 405 nm, λ_{em} = 687.8 nm, $^5D_0 \rightarrow {}^7F_0$) of three nanoaggregates C_1, C_2 and C_3 upon UV-C exposure for 0, 1 and 5 minutes (P ~200 µW/cm^2, λ ~185 nm) with (b) fine-scan SCM images demonstrating the multilevel $Sm^{3+} \rightarrow Sm^{2+}$ conversion. (c). SEM (BSED) images of the three small aggregates of ~2-3 nanocrystals. (d). The measured log-normal size distribution of aggregates, and the integrated photoluminescence intensity as a function of aggregate size for a collection of > 60 particles on the wafers. The size parameter is taken as the average length of the major and minor axes. (e). Experiment demonstrating that the write time can be reduced dramatically by at least 10 orders of magnitude, as demonstrated for the case of a bulk sample, by using an ArF excimer laser (30 ns pulse, ~30 mJ/cm^2 at 193 nm; blue trace) instead of the mercury UV lamp (red trace).

We also note that the photoluminescence intensity varies somewhat between the different nanoaggregates in e.g. Figure 4, due to the different sizes. The photoluminescence intensity as a function of nanoaggregate size is shown in Fig. 4(d) for a collection of more than 60 particles. The trend shows that the intensity simply increases with the cube of the particle size, i.e. with the volume of the sample. Figure 4(d) also shows the log-normal size distribution of the nanoaggregates measured on the silicon wafers. In practice the photoluminescence intensity should be similar between different pixels and further engineering would be required to ensure this. In particular, more uniform particles could be

Optics EXPRESS

prepared by using microemulsions and capping of the nanoparticles. Note that the nanoaggregates appear to have very similar SCM fluorescence images despite having very different geometries. This is primarily due to the resolution limits of the microscope and possibly slight misfocus on the sample.

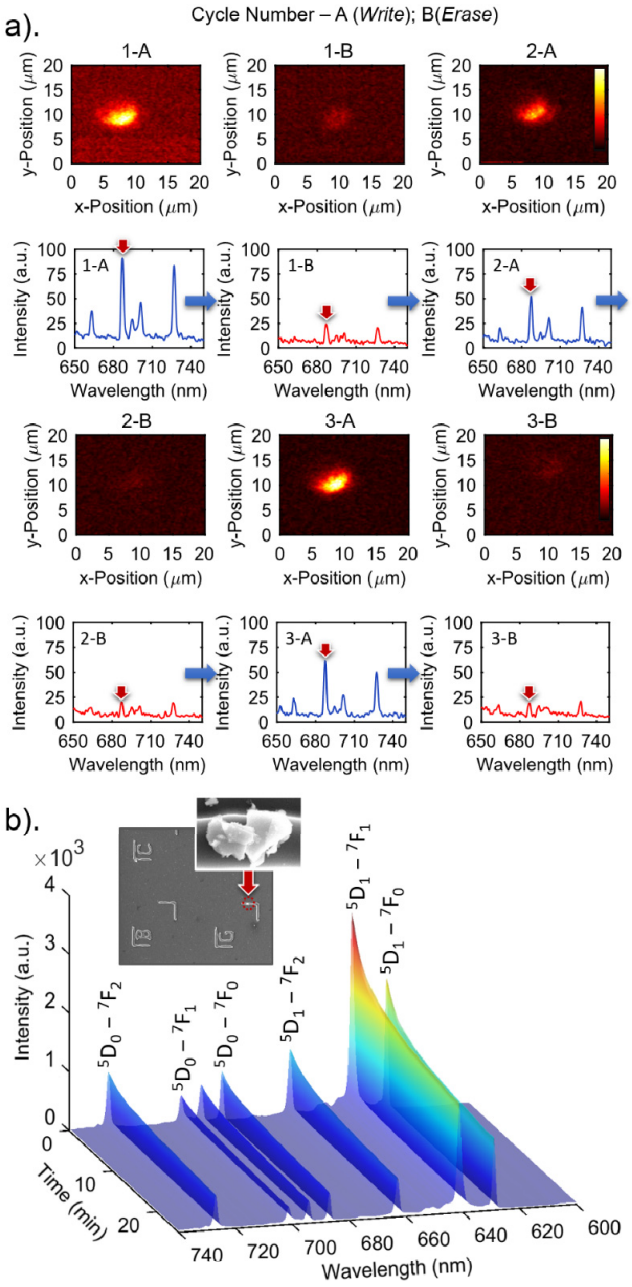

Fig. 5. (a). Rewritable data storage demonstration. The write-read-erase cycle is demonstrated three consecutive times on the nanoaggregate C_1. Shown are the 405 nm excited photoluminescence emission spectra (5s integration) and the SCM images after 1 mJ/cm^2 radiant exposure and with subsequent bleaching. (b). Typical Sm^{2+} to Sm^{3+} bleaching/erasure kinetics (P = 360 μW, t ~½ hr).

Optics EXPRESS

D. Rewritable optical data storage

A proof-of-concept of the repeatability of the write-read-erase cycle was subsequently demonstrated using the same wafer as in the previous result (specifically nanoaggregate C_1). Figure 5(a) demonstrates three consecutive write-read-erase cycles as shown by their SCM images and spectra. The 688 nm $^5D_0 \rightarrow {}^7F_0$ *f-f* transition shows no signs of weakening after these cycles as might be expected [19]. Many more cycles could be demonstrated if UV-grade optics were used to allow exposure of the sample via the microscope.

E. Single nanocrystal optical data storage

Whilst the previous results used small clusters of 2 or 3 individual crystals, the same behavior reported is observed when a single crystal can be isolated, albeit with lower signal strength. Figure 6 shows a basic result for the write-read-erase cycle of a single crystal (with its SEM image shown in the inset) for a 980 nm × 1400 nm crystal (third dimension of platelet is typically ~50 nm). This result provides a proof-of-concept of valence-state switching at the level of a single nanocrystal. We note that at least one dimension of the crystals is well and truly on the nanoscale.

Interestingly, in our results (especially Figs. 5(b) and 6), the 640 nm Sm^{2+} transition is unusually strong compared to what has been observed in the literature [19]. We observe that the intensities of the Sm^{2+} $^5D_1 \rightarrow {}^7F_J$ luminescence lines are in fact highly power-dependent and the $^5D_1 \rightarrow {}^7F_1$ line dominates for the high powers used for bleaching/erasure (2-photon process). In agreement with the literature, at the lower read-out powers the $^5D_0 \rightarrow {}^7F_0$ transition at 688 nm dominates [19, 22]. It appears that the higher powers lead to a build-up of population in the $^5D_1$ level, possibly by excited state absorption of the $^5D_0$ level or phonon saturation effects due to confinement by the nanocrystal. To the best of our knowledge this effect has never been reported elsewhere and it remains to be fully investigated and will be subject of a future publication. For this paper the main transition considered is at 688 nm, which for the modest read-out powers used (to avoid potential bleaching), dominates over the 640 nm signal.

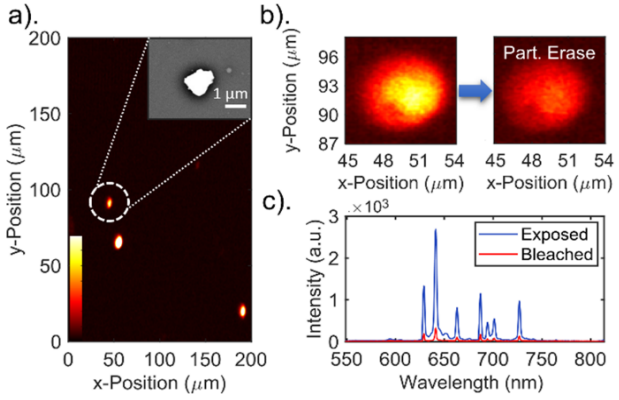

Fig. 6. Single nanocrystal switching. (a). The SCM image (λ_{ex} = 405 nm, λ_{em} = 687.8 nm, $^5D_0 \rightarrow {}^7F_0$) of the UV-C exposed single crystal with its SEM image shown in the inset. (b) The fine-scan SCM image upon UV-C exposure and after partial bleaching and (c) the corresponding spectra.

F. 2D & 3D super-resolution optical data storage

Whilst this paper has investigated optical data storage in nanocrystals of several hundred nanometers in size, it is expected that multilevel data storage would be possible for smaller nanocrystals down to 30 nm as-prepared by ball-milling [25, 26], provided e.g. there is higher signal collection efficiency, improved sample focusing, and multiple Sm^{2+} transitions from

Optics EXPRESS

the spectrum are measured simultaneously to increase the signal-to-noise ratio. Importantly, compared with nanocrystals prepared by co-precipitation, significantly higher Sm^{3+} concentrations of as much as 2 percent can be incorporated by the mechanochemical method which would allow for many more levels of data encoding. One challenge that was faced during a preliminary investigation of smaller ~30 nm nanocrystals was bleaching due to the increased excitation power used to achieve a strong read-out signal. As previously mentioned, the basic experimental setup and design used here could be improved considerably to avoid such bleaching by e.g. using a pulsed laser at around 420 nm for the read-out. Alternatively, two-photon absorption or upconversion based read-out employing a near-infrared laser could be used to excite the *f-f* fluorescence and hence avoid the bleaching issue all together. For this reason, much higher powers could be used for the read-out, overcoming the potential issue of low read-out signal.

It is believed that the data storage platform presented in this paper, using the BaFCl:Sm nanocrystals, could readily be extended to 2D, by embedding the nanocrystals into a flexible film (e.g. 5% Kraton^{TM}) [19], or by using various nanoparticle patterning techniques. It could also be readily extended to 3D which would permit ultra-high data densities of the order of many TB/cm^3 if hundreds or even thousands of levels are encoded. The platform would also permit fast parallel read-out as a result of the multibit encoding. In principle, super-resolution microscopy could also be used to minimize the writing pitch to about 30 nm, potentially allowing for up to PB/cm^3 data storage. To completely switch a 30 nm nanocrystal over its entire linear range, we calculate that a minute 5×10^{-12} J (5fJ) is needed. Such low energy requirements are particularly advantageous for applications in photonic chips.

4. Conclusions

In conclusion, optical data storage has significance well beyond providing more disk space; there are simply no viable alternatives for implementing massively parallel data access. Optical data storage could also have several other advantages over traditional storage technologies including greatly improved lifetime and lower energy requirements. This paper has demonstrated significant potential for multilevel optical data storage in nanocrystalline BaFCl:Sm^{3+} systems. It has provided proof-of-concept write-read-erase cycle demonstrations towards rewritable and stable multilevel optical data storage at the nanocrystal level. This approach could overcome many of the hurdles currently facing the implementation of 3D optical data storage, since it allows for high conversion efficiency and low read-out power, with high thermodynamic stability [27]. The results presented in this paper could lay the groundwork for future 2D and 3D data storage demonstrations with terabyte- or higher-level storage capacities exploiting the very unique properties of samarium-doped matlockites.

Funding

Australian Research Council (FL130100044).

Acknowledgments

Y. Ruan would like to thank D. W. Lau from RMIT University, Australia, and D. Simpson from University of Melbourne, Australia, for providing support with setting up the scanning confocal microscope. The authors also acknowledge the use of facilities at the Australian Research Council (ARC) Centre of Excellence for Nanoscale BioPhotonics.